Energy Capture Optimisation of 1-Degree-of-Freedom Pivoted Rigid Cylinders Undergoing Flow-Induced Vibration in Cross-Flows

A.D. Johnstone[1] and B. Stappenbelt[2]

[1]School of Mechanical, Materials and Mechatronic Engineering
University of Wollongong, Wollongong, New South Wales 2522, Australia

[2] School of Mechanical, Materials and Mechatronic Engineering
University of Wollongong, Wollongong, New South Wales 2522, Australia

Abstract

Experiments were conducted to study the energy capture performance of a pivoted rigid cylinder undergoing flow-induced vibration (FIV) in water cross-flow and assess its potential as a renewable energy technology. Two principle cylinder geometries were tested and in both cases the cylinder constrained to angular motion in the plane perpendicular to the cross-flow direction. In the first, a bare cylinder was allowed to undergo vortex-induced vibration (VIV), and in the second, non-rotating (NR) splitter-plates of two different lengths were fixed along the full length of the cylinder wake-side surface causing a galloping-type response from the cylinder. Various levels of damping ζ were applied to both the VIV and galloping cases and the magnitude of angular excursions and the time-averaged rate of energy capture measured. For each cylinder geometry/ζ combination tests were repeated at incremental steps between selected minimum and maximum reduced-velocity U_r. Results demonstrate that for a pivoted rigid cylinder the energy capture characteristic of the cylinder with NR splitter-plate (i.e. galloping) case is different to that of the bare cylinder undergoing VIV.

Introduction

When fluid flows are forced around a bluff object in their path the consequential changes to the flow resulting from the fluid/structure interaction can cause vibrations of the bluff object. The magnitude, frequency and character of the vibrations have much to do with the cross-sectional geometry and structural properties of the object and the degree to which it has freedom to move in various directions.

These cross-flow-induced vibrations are manifestly problematic for industrial and commercial applications affecting, for example, risers in the oil and gas industry, tubes in heat exchangers, design of tall slender buildings, power lines and bridge cabling. However, what if significant levels of the energy associated with these vibration phenomena could be harnessed? If so, such FIV could provide a useful energy source.

The two aforementioned cylinder geometries employed in this study have associated with them two different FIV phenomena: VIV and a galloping-type vibration, respectively, for the bare cylinder and the cylinders with a NR splitter-plate. For the case of translating motion (i.e. uniform displacement at all points along an object's axis) the VIV phenomenon for circular cylinders is extensively studied and documented.

For VIV of circular cylinders in cross-flows the fundamental relationships between vibration amplitude, frequency and the structural and fluid properties can be seen, for example, in Govardhan and Williamson [4], Khalak and Williamson [5,6] and Klamo, Willden and Graham [10]. For the bare pivoted circular cylinder there are studies investigating the FIV behaviour e.g.

[1,3,7,9]. However, to the present author's knowledge the FIV behaviour of pivoted rigid circular cylinders with NR wake splitter-plates has not been explored.

The effects of damping on circular cylinder structures undergoing FIV in cross-flows has been investigated (see e.g. Blevins and Coughran [2] and Leonard and Roshko [8]). However, the focus of these papers is the effect of the applied damping on the nature of the cylinder vibrations, not the degree to which energy is extracted from the cross-flow. The energy extraction potential of pivoted rigid circular cylinders undergoing FIV is the topic of the present study.

Experiment Apparatus and Methodology

The experiments were conducted at the University of Wollongong SMART Building wavetank facility. The wavetank is a free-surface tank with water as the working fluid and dimensions of length L_{tank} = 33m, width w = 1m and overall height $H \sim$ 1m (the coordinate conventions corresponding to the tank length, width and height, respectively, are assumed the x-, z- and y-directions). During the experiments the water in the tank was still and cross-flow velocity relative to the circular cylinders was achieved using a towing carriage powered by an electric motor running the full length of the tank. Thus, owing to the experiment arrangement, and the allowance of sufficient intervals between successive tests, the turbulence levels of the fluid 'upstream' of the cylinder during the experiments was negligible. To constrain the cylinder motion to the plane normal to the relative flow direction the cylinder was coupled to a shaft with the shaft axis aligned to the towing direction and running on a low-friction pillow block bearing pair mounted on the towing carriage. By this arrangement the test cylinder was pivoted about its upper end with the pivot point located approximately 0.20m above the free-surface of the water. The carriage itself runs along the wavetank frame and has an towing speed adjustable across the range 0m/s < U < 1.4m/s.. Figure 1 depicts the key features of the experiment arrangement including notation.

Bare Cylinder and Cylinders with Splitter-Plates

The VIV and the majority of the galloping (i.e. cylinder with splitter-plate) tests employed a smooth circular cylinder of outer diameter D = 0.044m and hollow carbon fibre (CF) material with overall length L_{cyl} = 0.827m as the main part of the test specimen. Thus the aspect ratio of the CF tube section was L_{cyl}/D = 18.8. A hollow aluminium tube of outer diameter d = 0.025m was inserted 0.10m into the upper end of the CF tube and the two tubes fitted together using solid watertight rubber grommets. The aluminium tube provided a stable, rigid joint at the interface of the test cylinder and carriage mounted pivot shaft. No end-plates were fitted to either the upper or lower ends of the cylinder. Another cylinder of outer diameter D = 0.090m and made of
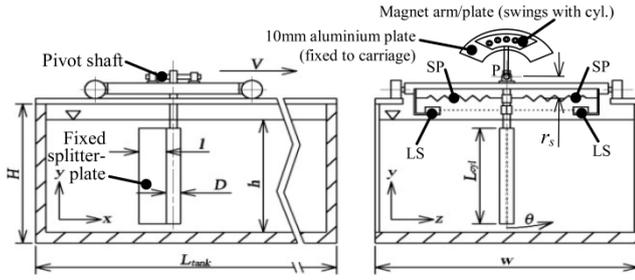
Figure 1. Schematic of experiment apparatus. Items SP and LS denote, respectively, the spring-sets and the laser displacement sensors used to measure the cylinder motion. Note: Damping components are not shown on the x-y view; no splitter-plate attached to the cylinder for VIV tests.

Inertia of cylinder	I	(kg.m^2)
Natural frequency of cylinder in water	f_{nw}	(Hz)
Inertia ratio	I^*	I/I_d
Moment ratio	M^*	M/M_d
Torque ratio	T^*	$(M+s_\theta)/M_d$
Normalised angle of cylinder motion	θ^*	θ/θ_{cyl}
Reduced-velocity	U_r	$U/(f_{nw}D)$

Table 1. Notation and non-dimensional parameters. Note: All inertia and moment values are calculated about the pivot axis of the cylinder; f_{nw} corresponds to the natural frequency of the cylinders in quiescent water. For a system without springs $T^* = M^*$ (see equation 3).

hollow PVC tube was also used for the cylinder with splitter-plate tests. An inner aluminium tube identical to that used for the CF tubes was again employed.

All splitter-plates spanned the full length of the cylinders such that the dimension of the splitter-plates aligned with the cylinder axis was equal to L_{cyl} in all cases (see figure 1). Two different splitter-plate lengths were employed: $l = 0.5D$ and $1.0D$, where l is the splitter-plate dimension measured perpendicular to the cylinder axis (see figure 1). In the case of the 44mm diameter cylinders the splitter-plates were of 1.0mm thick CF sheet supported at the joint with the cylinder by gussets made from CF fabric. For the 90mm diameter PVC cylinder 1.8mm thick aluminium sheet was used. This was attached by cutting along the splitter-plate edge making contact with the PVC tube around 16 equispaced slots of approximately 15mm length, each slot cut in the direction parallel to the l dimension. The tabs created by the cut slots were alternately bent in opposite directions, curved slightly to form a neat fit to the outer surface of the PVC tube and then glued and riveted to the PVC cylinder.

The angular excursion of the pivoted cylinder has been defined in terms of a normalised angular excursion $\theta^* = \theta/\theta_{cyl}$, where θ is the angular orientation of the cylinder axis from vertical. The cylinder angle θ_{cyl} is the angle made between the cylinder axis and a line taken from the pivot location P to a point on the circumference at the end of the cylinder farthest from the pivot.

In each experiment run the magnitude of the angular excursion θ of the pivoted cylinder was determined through averaging all the peaks of the vibration response data.

Structural Properties

Free-decay tests were employed to ascertain the degree of damping associated with the pillow-block bearings. Values for the damping ratio ranged between $\zeta \sim 0.005$ to $\zeta \sim 0.0005$ corresponding to cylinder angular excursions of $\theta^* \cong 7$ and $\theta^* \to 0$, respectively.

For each experiment extension springs were used to control the system stiffness. Two opposing spring-sets of equal stiffness were mounted horizontally and in-plane with the y-z plane with

D (m)	Splitter-plate length (l/D)	M^*	I^*	f_{nw} (Hz)	ζ
0.044	NA	0.040	0.241	0.54	Nil, 0.036, 0.071, 0.143 & 0.300.
0.044	0.5	0.200	0.391	0.30	0.025, 0.049 & 0.099.
0.044	0.5	0.200	0.656	0.30	0.024, 0.039, 0.057, 0.070 & 0.092.
0.044	0.5	0.335	0.847	0.30	0.020, 0.044, 0.060 & 0.084.
0.090	0.5	0.191	0.292	0.17	0.017, 0.030, 0.043, 0.053, 0.065 & 0.078.
0.044	1.0	0.224	0.399	0.21	0.035, 0.070, 0.088 & 0.105.

Table 2. Test regimes and cylinder properties. Note: VIV and galloping are considered, respectively, the dominant FIV of row 1 and rows 2–6.

one end attached to a collar on the aluminium tube of the test cylinder and the other to the towing carriage (see figure 1). The offset r_s of the spring-sets and associated carriage connection points from the cylinder pivot location P was adjustable in order to control the angular stiffness s_θ associated with the spring-set.

For n number of springs, each with equal stiffness k, the force exerted by the spring-set is

$$F = nkd \quad (N), \tag{1}$$

where, d is the linear displacement of one end of the spring-set, the other end fixed in place.

Thus, the total stiffness of the spring-set k_{total} is defined as

$$k_{total} = \frac{F}{d} = nk \quad (N/m). \tag{2}$$

Under the assumption of small angular motions (i.e. $\sin\theta \sim \theta$), the effective angular stiffness of the spring-set is then

$$s_\theta = k_{total} \cdot r_s^2 \quad (N.m/rad). \tag{3}$$

Figure 3 portrays the experiment arrangement noting c_b and c_m to be the centre-of-buoyancy and centre-of-mass, respectively, each shown at arbitrary locations along the cylinder.
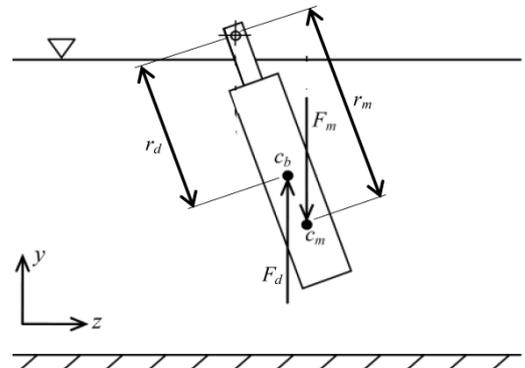

Figure 3. Experiment arrangement of the pivoted circular cylinder.

The moment-ratio M^* is considered herein to be the ratio of the moment acting about the cylinder pivot working to restore the cylinder to vertical alignment – exclusive of the applied stiffness of the spring sets - to the moment causing the cylinder to diverge from vertical alignment. For the orientation of the cylinder in this study (see figure 3) this corresponds, respectively, to the moment associated with the body mass M (restoring moment) and the

buoyancy moment associated with the fluid displaced by the cylinder M_d (diverging moment). Hence,

$$M^* = \frac{M}{M_d} = \frac{F_m \cdot r_m \cdot \sin\theta}{F_d \cdot r_d \cdot \sin\theta} = \frac{F_m \cdot r_m}{F_d \cdot r_d}. \qquad (4)$$

Accounting for the effects of cylinder mass and buoyancy the overall stiffness of the pivoted cylinder (assuming $\sin\theta \sim \theta$) is

$$k_\theta = s_\theta + M - M_d \quad \text{(N.m/rad)}. \qquad (5)$$

The inertia-ratio I^* is the ratio of the mass-moments of inertia about the cylinder pivot associated with the distribution of the cylinder mass I and the fluid displaced by the cylinder I_d.

$$I^* = \frac{I}{I_d} \qquad (6)$$

Applied Damping

Damping linearly proportional to the angular velocity of the cylinder was achieved through the use of magnetic damping. To do so, a 10mm thick aluminium plate was fastened to the towing carriage. Also, a CF sheet carrying a magnet array was attached to a CF tube extension rigidly coupled to the inner aluminium tube of the main cylinder (see figure 1). The level of damping c_θ was set through adjustment of the air gap between the magnets and the stationary aluminium plate.

For all tests the added-inertia coefficient C_a matching the theoretical natural frequency in water $f_{nw\text{-}theory}$ calculated by equation (7) to f_{nw} measured (see table 2) was determined. Note: Added inertia, $I_a = C_a \times I_d$.

$$f_{nw-theory} = \frac{1}{2\pi} \sqrt{\frac{k_\theta}{I+I_a}} \quad \text{(Hz)} \qquad (7)$$

For the cylinders with splitter-plates of length $l = 0.5D$ the C_a values are presented in figure 4.
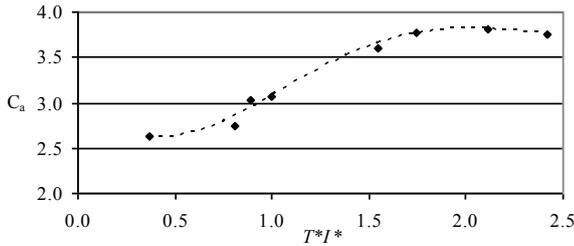
Figure 4. Added inertia coefficient (C_a) that gives $f_{nw\text{-}theory} = f_{nw}$ for the cylinders with splitter-plates $l = 0.5D$. Note: Data points are from both D = 44mm & 90mm cylinders.

In order to determine the damping ratio ζ of each test the appropriate C_a value was incorporated into equation (8).

$$\zeta = \frac{c_\theta}{2\sqrt{k_\theta (I+I_a)}} \qquad (8)$$

The efficiency ε of energy extraction from the flow was defined as the ratio of the time-averaged rate of energy extracted by the applied damping to the power of the flow incident on the frontal area of the cylinder i.e.

$$\varepsilon = \frac{\overline{P_{out}}}{\frac{1}{2}\rho_w D L_{cyl} U^3} \qquad (9)$$

where ρ_w is the density of water (kg/m^3), and
U is the carriage velocity i.e. cross-flow velocity (m/s).

Experiment Results

Vortex-Induced Vibration (VIV)

The outcomes of the VIV tests with applied damping are presented in figure 5 and figure 6. The shape of the cylinder angular vibrations θ^* versus U_r response (see figure 5) accords

well with the trend often seen in VIV i.e. a peak magnitude at $U_r \sim 5$ and gradual reduction in θ^* at larger U_r values. The no-damping case forms the outer envelope of θ^* and consistent reduction in θ^* with increased damping occurred across the entire U_r range tested.
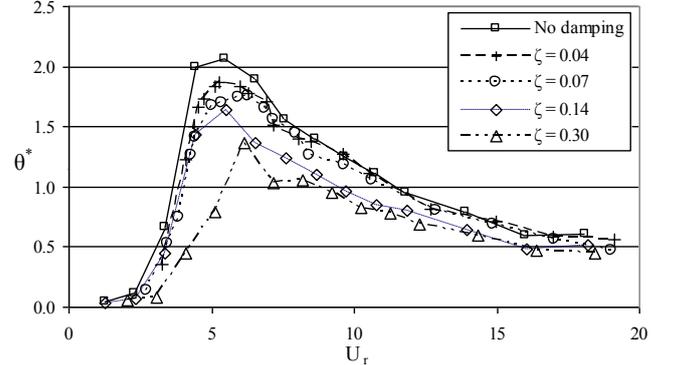
Figure 5. Average magnitude of VIV angular vibrations θ^* versus U_r. Pivoted cylinder properties: D=0.044m, L=0.824m, M^*=0.040, I^*=0.241.

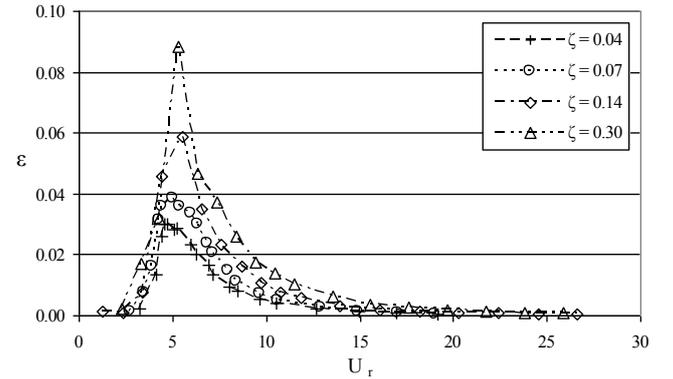Figure 6. Efficiency (ε) of energy extraction from VIV versus U_r. Pivoted cylinder properties: D=0.044m, L=0.824m, M^*=0.040, I^*=0.241.

Converse to the magnitude of θ^*, the peak VIV efficiency continued to increase with greater ζ (see figure 6). This is an indication that at larger ζ than tested (i.e. $\zeta > 0.30$) further increase in efficiency is likely. Eventually, as a consequence of its limiting effect on θ^*, it is anticipated that at a sufficiently large value of ζ the maximum possible ε will be attained.

It is noted that the present VIV results are limited to a single combination of the cylinder structural properties and geometry i.e. M^*, I^* and L/D. It is well established that for cylinders undergoing VIV generally, both the shape and magnitude of the vibration response are linked to the structural properties of the cylinder. Therefore, given the evident link herein between θ^*, ζ and ε, the influence of the structural properties may also extend to the VIV energy extraction performance. Hence, energy extraction performance superior to the results of the present work may well be possible for VIV of pivoted rigid circular cylinders.

Galloping - Cylinder with Non-Rotating Wake Splitter-Plate

Similar to the VIV case the energy extraction characteristic of the cylinders with NR splitter-plates exhibit a rise to a peak efficiency occurring at a particular U_r (see figure 7). Furthermore, like the VIV case the peak is then followed by a steady reduction in efficiency as U_r increases further. Where the VIV and splitter-plate cases differ, however, is in the overall shape and breadth of the ε versus U_r curves. Unlike the pointed peak present in the VIV ε curve the splitter-plate curves are more continuous and smooth across the peak in ε. In addition, the U_r range at which there exists ε of similar order of magnitude as the ε peak – say $U_r\sigma(\varepsilon)$ – greatly exceeds that of the VIV case.

Differences exist between the energy extraction characteristics of

the two splitter-plate cases. Figure 7 shows that the increase in splitter-plate length from $l = 0.5D$ to $l = 1.0D$ flattened out the ε versus U_r curve (increasing U_r of (ε)) and, additionally, reduced the efficiency at any given level of damping. For example, at $\zeta \sim 0.1$ in figure 7 the $l = 0.5D$ to $l = 1.0D$ cylinders have peak efficiencies of $\varepsilon \sim 0.038$ and $\varepsilon \sim 0.024$, respectively (note that the structural properties M^* and I^* of the $l = 0.5D$ to $l = 1.0D$ cylinders are closely matched).

With reference to figure 8, the influence of the structural properties M^*, I^* and k_θ on the peak efficiency is best understood in terms of the combined effect these properties have on the damping ratio value. Firstly, the added-inertia coefficient $C_a = f(T^* \times I^*) = f((M^* + s_\theta/M_d) \times I^*)$ (see figure 4) and, hence, the structural properties influence the value of the added-inertia I_a. Secondly, ζ is then determined according to equation (8) and, lastly, the magnitude of peak ε is dependent on the ζ.
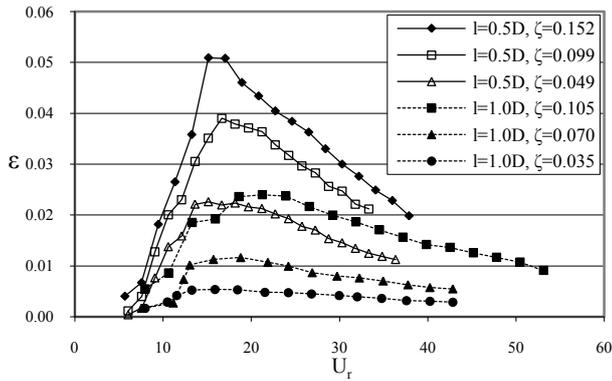

Figure 7. Energy extraction characteristics of galloping cylinders with $l = 0.5D$ and $l = 1.0D$ splitter-plates - shown in terms of ε versus U_r; Pivoted cylinders with splitter-plates properties: D=0.044m, L=0.827m, Carbon fibre. $l = 0.5D$: $M^* = 0.200$, $I^* = 0.391$; $l = 1.0D$: $M^* = 0.224$, $I^* = 0.399$.
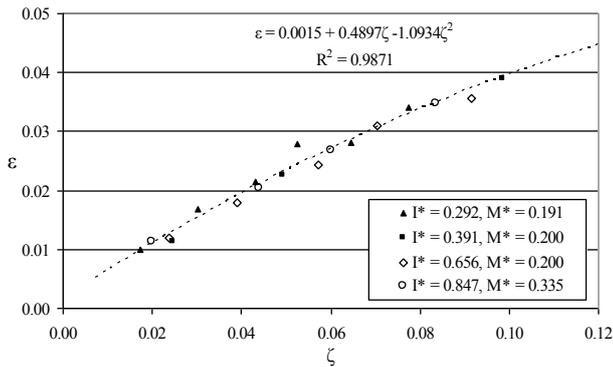

Figure 8. Peak energy extraction efficiency of cylinders with splitter-plate $l = 0.5D$.

Lastly, the energy extraction efficiencies of the cylinders undergoing VIV and galloping are presented together in figure 9. The data suggests a peak efficiency for the $l = 0.5D$ cylinder to be limited to approximately $\varepsilon = 0.06$. For the $l = 1.0D$ case there is the possibility of greater ε at larger ζ than tested. However, at sufficiently large ζ the $l = 1.0D$ case is expected to exhibit similar limiting ε behaviour as the $l = 0.5D$ case.

Conclusions

When considering FIV of a pivoted rigid cylinder and assuming two distinct geometry options (i.e. bare cylinder or cylinder with NR splitter-plate), the study outcomes allow for system design towards maximising energy capture from the cross-flow. Application of VIV energy capture is limited to a narrow U_r band. This is not problematic from an installation perspective

however provided a reasonably stable flow velocity exists. In contrast to VIV the energy capture range of the cylinders with splitter-plates extends over a broader U_r range. For pivoted rigid circular cylinders the present results indicate the energy extraction potential of VIV to be superior to that of the cylinders with splitter-plates.
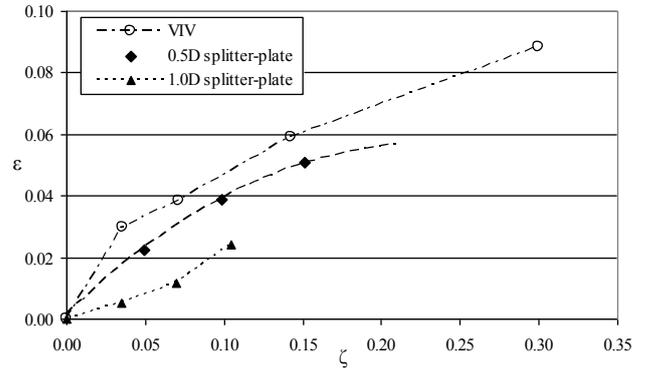

Figure 9. Energy extraction efficiency of bare cylinder and cylinders with splitter-plates $l = 0.5D$ and $l = 1.0D$. Note: VIV data are peak ε from figure 6; Splitter-plate data points are peak ε from figure 7; Splitter-plate $l = 0.5D$ curve is the trendline fit equation of figure 8.

References

[1] Balasubramanian, S., Skop, R.A., Haan Jr, F.L. & Szewczyk, A.A., Vortex-Excited Vibrations of Uniform Pivoted Cylinders in Uniform and Shear Flow, *Fluid. Struct.*,**14**, 2000, 65-85.

[2] Blevins, R.D. & Coughran, C.S., Experimental Investigation of Vortex-Induced Vibration in One and Two Dimensions with Variable Mass, Damping, and Reynolds Number, *Fluid. Eng.*,**131**, 2009, 1012021-1012027.

[3] Flemming, F. & Williamson, C.H.K., Vortex-Induced Vibrations of a Pivoted Cylinder, *Fluid. Mech.*,**522**, 2005, 215-252.

[4] Govardhan, R. & Williamson, C.H.K., Modes of Vortex Formation and Frequency Response of a Freely Vibrating Cylinder, *Fluid. Mech.*,**420**, 2000, 85-130.

[5] Khalak, A. & Williamson, C.H.K., Fluid Forces and Dynamics of a Hydroelastic Structure with Very Low Mass and Damping, *Fluid. Struct.*,**11**, 1997, 973-982.

[6] Khalak, A. & Williamson, C.H.K., Motions, Forces and Mode Transitions in Vortex-Induced Vibrations at Low Mass-Damping, *Fluid. Struct.*,**13**, 1999, 813-851.

[7] Kheirkhah, S., Yarusevych, S. & Narasimhan, S., Orbiting Response in Vortex-Induced Vibrations of a Two-Degree-of-Freedom Pivoted Circular Cylinder, *Fluid. Struct.*,**28**, 2012, 343-358.

[8] Klamo, J.T., Leonard, A. & Roshko, A., The Effects of Damping on the Amplitude and Frequency Response of a Freely Vibrating Cylinder in Cross-Flow, *Fluid. Struct.*,**22**, 2006, 845-856.

[9] Voorhees, A., Dong, P., Atsavapranee, P., Benaroya, H. & Wei, T., Beating of a Circular Cylinder Mounted as an Inverted Pendulum, *Fluid. Mech.*,**610**, 2008, 217-247.

[10] Willden, R.H.J. & Graham, J.M.R., Three Distinct Response Regimes for the Transverse Vortex-Induced Vibrations of Circular Cylinders at Low Reynolds Numbers, *Fluid. Struct.*,**22**, 2006, 885-895.